Nanocompuestos de ácido poliláctico y policaprolactona para la regeneración tisular subdérmica

Polylactic acid and polycaprolactone nanocomposites for subdermal tissue regeneration

Jorge Iván Castro[1], Andrés Felipe Niebles Navas[2], Carlos-Humberto Valencia-Llano[3], Diego López Tenorio[3] and Carlos David Grande-Tovar[4] *

1. Magister, Research Professor, Universidad del Valle, Tribology, Polymers, Powder Metallurgy and Solid Waste Transformations Research Group, Cali-Colombia.
2. Chemist student, Universidad del Atlántico, Grupo de Investigación de Fotoquímica y Fotobiología, Puerto Colombia- Colombia.
3. PhD, Research Professor, Universidad del Valle, Grupo Biomateriales Dentales, Escuela de Odontología, Cali-Colombia.
4. PhD, Chemist, Research Professor, Universidad del Atlántico, Grupo de Investigación de Fotoquímica y Fotobiología, Puerto Colombia- Colombia.

* Correspondence: carlosgrande@mail.uniatlantico.edu.co

Cite this article as: J. Castro, A.Niebles, C.-H. Valencia-Llano, D .Lopez, C. D. Grande-Tovar "Nanocompuestos de ácido poliláctico y policaprolactona para la regeneración tisular subdérmica", Prospectiva, Vol. 22 N° 2 2024.

Recibido: 19/01/2024 / Aceptado: 16/05/2024

http://doi.org/ 10.15665/rp.v22i2.3432

ABSTRACT

Tissue defects in the skin caused by accidents or diseases have opened different avenues of research for constructing new biocompatible materials. In this sense, we present the synthesis of four composite-type membranes based on polylactic acid (PLA), polycaprolactone (PCL), ginger essential oil (GEO), and zinc oxide nanoparticles (ZnO-NPs) for subdermal tissue regeneration. FTIR, XRD, TGA, and DSC performed chemical characterization. Incorporating GEO and ZnO-NPs in the formulations showed an increase of the C-O-C band and a decrease at 1722 cm-1, corresponding to the interaction between the C=O group and the ZnO-NPs. The (TGA) and (DSC) confirmed incisions in the backbone of the polymeric matrix due to the interaction on the carbonyl group by the ZnO-NPs. Moreover, the introduction of GEO in the formulations decreases the thermal stability due to the introduction of intermolecular spaces. The morphological study by scanning electron microscopy (SEM), except for F1, showed a porous microstructure confirming the interaction between the polymeric matrix's ZnO-NPs, GEO, and carbonyl groups, beneficial for tissue regeneration. Examination of the implanted membranes by histological analysis demonstrated their biocompatibility and biodegradability 60 days after implantation. Simultaneous degradation and formation of type I collagen fibers, with increased blood vessels and inflammation, indicate a highly biocompatible and resorbable material.

Keywords: *biocompatible materials; polymer composites; tissue defects; ZnO-NPs.*

RESUMEN

Los defectos tisulares en la piel causados por accidentes o enfermedades han abierto diferentes vías de investigación para la construcción de nuevos materiales biocompatibles. En este sentido, presentamos la síntesis de cuatro membranas de tipo composite basadas en ácido poliláctico (PLA), policaprolactona (PCL), aceite esencial de jengibre (GEO) y nanopartículas de óxido de zinc (ZnO-NPs) para la regeneración de tejido subdérmico.La caracterización química se realizó mediante FTIR, XRD, TGA y DSC. la incorporación de GEO y ZnO-NPs en las formulaciones, demostro un aumento de la banda C-O-C así como la disminución de la banda a 1722 cm-1 correspondiente a la interacción entre el grupo C=O y las ZnO-NPs. El (TGA) y (DSC) confirmaron incisiones en la espina dorsal de la matriz polimérica debido a la interacción sobre el grupo carbonilo por parte de las ZnO-NPs. Además, la introducción de GEO en las formulaciones disminuye la estabilidad térmica, debido a la introducción de espacios intermoleculares. El estudio morfológico mediante microscopía electrónica de barrido (SEM), excepto en el caso de F1, mostró una microestructura porosa que confirma la interacción entre las ZnO-NPs, la GEO y los grupos carbonilo de la matriz polimérica, beneficiosa para la regeneración tisular. El examen de las membranas implantadas mediante análisis histológico demostró su biocompatibilidad y biodegradabilidad 60 días después de la implantación. La degradación simultánea y la formación de fibras de colágeno de tipo I, con el aumento de los vasos sanguíneos y la inflamación, indican un material altamente biocompatible y reabsorbible.

Palabras clave: *materiales biocompatibles; compuestos poliméricos; defectos tisulares; ZnO-NPs.*

1. Introduction

The skin is the largest organ of the human body, whose primary function is to act as a barrier against the various surrounding environmental factors such as ultraviolet radiation and microbial infections. Other skin functions are thermoregulation, touch, production, and storage of biomechanisms (vitamin D, keratin, lipids, and protein) [1,2]. Skin defects due to trauma, such as burns, or diseases such as diabetes, in many cases, affect the above functions, leading to amputations and even death. In this sense, there is a need to promote the regeneration of damaged skin tissue through methods of inducing active wound healing. To this end, scaffolds based on polymeric systems, which can support the generation of new and functional tissue [3,4], have been explored.

The different scaffolds are mainly constituted with variations between synthetic polymers such as polycaprolactone, polylactic acid, polyurethane, polydimethylsiloxane, or polyethersulfone with natural biodegradable polymers such as chitosan [5]. Additionally, combinations have been found with various nanoparticles such as mineral [6], carbon-based [7], or metallic nanoparticles. The reason for these combinations is to obtain the benefits of each component by enhancing cell adhesion and mechanical, thermal, biodegradable, and biocompatible properties [8]. Therefore, the natural and synthetic components mixture provides a suitable tissue regeneration medium as they often possess extracellular matrix components [9].

Polylactic acid (PLA) is derived from lactic acid, obtained through the fermentation of various biological sources containing lactic acid bacteria. This polymer serves as a substitute for olefinic plastics. The availability of natural resources, biocompatibility, and biodegradability have generated significant interest in bio-medical applications [10]. Consequently, PLA finds utility in tissue engineering to restore or enhance tissue functionality by combining bioactive molecules, cells, and scaffolds. PLA's biocompatible properties enable the creation of scaffolds with optimal architectures for regenerating intricate tissues [11].

On the other hand, polycaprolactone is a thermoplastic, biodegradable, and biocompatible synthetic polymer derived from ε-caprolactone. PCL exhibits an amorphous phase at room temperature and a melting point typically at 55–70 °C [12]. PCL synthesis involves a ring-opening mechanism facilitated by a catalyst [13].

However, PCL/PLA blends face mechanical challenges at elevated temperatures due to PLA's slow crystallization rate, which is attributed to the enantiomeric mixture of its major component (the L isomer) and its glass transition temperature, typically falling between 55 and 65 °C [14,15]. Therefore, adding plasticizers, such as essential oils or nanofillers like inorganic nanoparticles, has been suggested to address these issues related to low elongation and toughness properties.

Zinc oxide nanoparticles (ZnO-NPs) represent a viable class of semiconductors known for their exceptional chemical stability and cost-effectiveness, and their safe application has garnered approval from the Food and Drug Administration (FDA) [16]. These nanoparticles can be synthesized through various techniques, including precipitation [17], the sol-gel method [18], spray pyrolysis [19], thermal decomposition [20], and forced solvolysis [21]. ZnO-NPs, characterized by their chemical stability, biocompatibility, and antimicrobial properties against a broad spectrum of microorganisms such as Escherichia coli, Pseudomonas aeruginosa, and Staphylococcus aureus [22,23], have become an attractive choice for multiple applications spanning textiles [24], packaging [25], and medicine [26]. Numerous methodologies have been explored to assess the impact of ZnO-NPs in polymer composites, focusing on creating PLA/ZnO nanocomposites. These nanocomposites have also exhibited remarkable antimicrobial efficacy against bacteria like E. coli, S. aureus, and Klebsiella pneumoniae [27–30].

Essential oils comprise volatile molecules with safe and promising antimicrobial properties that increase polymeric matrices' physical properties [31]. Zingiber officinale Roscoe or ginger essential oil (GEO) contains components such as α-zingiberene, β-sesquiphellandrene, α-curcumene, and camphene [32]. Generally, this extract has been used to manufacture films to study antibacterial activity using natural or synthetic polymers

such as chitosan or polyvinyl alcohol. Various biopolymers, such as gelatin or carboxymethylcellulose, have also produced composite films with GEO [33–35].

In a previous endeavor, our research group crafted four membranes composed of chitosan (CS), tea oil essential (TTEO), and polyvinyl alcohol (PVA). TTEO was utilized as a plasticizer in these membranes. Our investigation revealed that incorporating TTEO enhanced biodegradability and biocompatibility, reducing inflammatory responses and nearly complete bioabsorption within 90 days of implantation [36]. Nevertheless, to our knowledge, no prior studies have explored the in vivo assessment of the biocompatibility of zinc oxide nanoparticles and GEO within a polymeric matrix of PLA/PCL. Such an exploration can potentially enhance these materials' biological response and stability.

Hence, our study sought to preliminarily evaluate the biocompatibility of membranes composed of PLA/PCL/GEO/ZnO-NPs through subdermal implantation in Wistar rats. The outcomes indicated an accelerated resorption process and the absence of an aggressive inflammatory response, thereby underscoring the promising application of these materials in tissue engineering.

2. Materials and Methods

2.1. Materials

All reagents used in this investigation were used without any additional purification process. The 6800-layer PCL was obtained from the Perstorp Company (Limited of Warrington, UK) with a molecular weight and fluence rate of 8000 g/mol and 3g/10min, respectively. PLA was obtained from Nature Works Company (Minnetonka, Minnesota, USA) with a molecular weight of 200000 Da and a content of 2% attributed to the D isomer. For the synthesis of the ZnO-NPs, reagents such as ZnCl2 80%, 99% sodium hydroxide, and 99.8% 2-propanol were provided by Merck of Burlington (MA, USA).

2.2. Synthesis of ZnO-NPs

Previous methodologies carried out the synthesis of ZnO-NPs [37]. Briefly, a 0.2M solution of ZnCl2 was mixed with a 5M NaOH solution, stirring at 90°C. The residue was washed with plenty of water and ethanol to remove NaCl. Centrifugation at 5000 rpm for 20 min and washing with 2-propanol in triplicate was used for purification. Finally, the ZnO-NPs were calcined at 250°C for five hours [38].

2.3 Composition of ginger essential oil (GEO)

Ginger essential oil (Zingiber officinale, GEO) was acquired from Marnys, Madrid, Spain. The composition of GEO was assessed using gas chromatography-mass spectrometry (GC-MS) (Table S1). Hydrocarbons ranging from C6 to C25 were employed as reference compounds in an AT 6890 series plus gas chromatograph (Agilent Technologies, Palo Alto, CA, USA) coupled with a mass selective detector (Agilent Technologies, MSD 5975). A DB-5MS column (J & W Scientific, Folsom, CA, USA) with a 5% phenyl-95% dimethylpolysiloxane (Ph-PDMS) phase was used as a separation phase. Identification was based on the retention indexes (RI) with the Adams database (Wiley, 138) and NIST05 (Agilent, Santa Clara, California, United States).

2.4. Preparation of the PLA/PCL/GEO ZnO-NPs membranes

We prepared the membranes of PLA/PCL/GEO/ZnO-NPs nanocomposite based on previous methodologies [39]. All the nanocomposite formulations with a final total solids content of 4% were prepared using the drop-casting method. The ZnO-NPs were ultrasonicated using an ultrasonic bath (Branson, Madrid, Spain) in chloroform at 300 mg/ml concentration for two hours. Then, each component was dissolved in chloroform and mixed according to Table 1. Finally, the mixture obtained was taken to an ultrasonic bath (Branson, Madrid, Spain) to eliminate the bubbles in the solution. Additionally, the mixture was transferred on glass molds to a preheated oven at 40°C ± 0.2 to obtain the PLA/PCL/GEO/ZnO-NPs membranes.

Tabla 1. Formulación de las membranas de PLA/PCL/GEO/ZnO-NPs

Components	PCL (%)	PLA (%)	GEO (%)	ZnO-NPs (%)
F1	30	70	0	0
F2	27	70	0	3
F3	20	70	10	0
F4	17	70	10	3

Table 1. Formulation of PLA/PCL/GEO/ZnO-NPs membranes.

2.5. Characterization of the ZnO-NPs

The characterization of ZnO-NPs has been reported elsewhere [6].

2.6. Characterization of PLA/PCL/GEO/ZnO-NPs membranes

2.6.1 X-ray diffraction (XRD) and Fourier transform infrared spectroscopy (FTIR).

Crystal structure analysis was carried out using a PANalytical X0Pert PRO diffractometer (Malvern Panalytical, Jarman Way, Royston, UK) with a Cu anode at a wavelength of Kα1 (1.540598 Å). Diffractograms were taken in the 5-50° range with a scan speed of 2.63 s, scan rate of 2 degrees/min, and a step size of 0.01°. Attenuated Total Reflectance-Fourier Transform Infrared Spectroscopy (ATR-FTIR) investigated functional groups and molecular interactions in the 500-4000 cm-1 range. The spectra were acquired using an FT-IR-8400 instrument (Shimadzu, Kyoto, Japan) with a spectral resolution of 4 cm-1 and 32 scans.

2.6.2 Thermal Analysis of the PLA/PCL/GEO/ZnO-NPs membranes

Thermogravimetric analysis (TGA) was conducted on a NETZSCH TG 209 F1 Libra instrument from Metter Toledo, Schwerzenbach, Switzerland. The samples were heated over an Al2O3 crucible from 25-800°C at 10°C/min under nitrogen. Thermodynamic properties were obtained using differential scanning calorimetry (DSC) with a DSC1/500 instrument (Mettler Toledo, Schwerzenbach, Switzer-land) in a nitrogen atmosphere. For the thermal analysis, 25 - 250°C heating was carried out at 10°C/min. In this way, properties such as glass transition temperature (Tg) calculated with the midpoint of the transition and melting temperature (Tm) were obtained from the endothermic peaks. Finally, the crystallization temperature (Tc) was calculated from the exothermic peak. The data obtained from the scanning calorimetry were processed, considering the second heating to eliminate the polymers' thermal memory. TA Instruments Universal Analysis Software 2000 version 4.5A was used to determine the above properties.

2.6.3 Scanning Electron Microscopy

The PLA/PCL/GEO/ZnO-NPs nanocomposite microstructure was performed on a JEOL JSM-6490LA instrument (Musashino, Tokyo, Japan) operated in the secondary electron mode at 20 kV. The samples were impregnated with a gold layer to increase the conductivity.

2.7 Surgical preparation of biomodels

The primary objective of this study was to evaluate the biocompatibility of the four formulations through in vivo testing using a subcutaneous implantation method. This design enabled the simultaneous implantation of multiple samples in biomodels, and their responses were examined over time [40]. The experiment adhered to the guidelines outlined in UNE: 10993-6 (Biological evaluation of medical devices—Part 6: Tests for local effects after implantation. ISO 10993-6: 1994). For the experiment, three biomodels, five-month-old male Wistar rats weighing 380 grams, were chosen from the Intermediate Laboratory of Preclinical Research and Biotherium (LABBIO) at Universidad del Valle.

Following the incision of the biomodels, various blocks were implanted to evaluate biocompatibility [41]. Sedation was achieved with Ketamine (70 mg/kg, Blaskov Laboratory, Bogotá, Colombia) and Xylazine (30 mg/

kg, ERMA Laboratories, Celta, Colombia). The implantation site was isolated and sterilized. Local anesthesia used Lidocaine with epinephrine (2%). Four 5 mm long incisions were made along the dorsal midline, with a one-centimeter interval. Subcutaneous pocket-type preparations, 2 cm deep, were then created on the right side using hemostatic forceps. After a 60-day implantation period, the biomodels were humanely euthanized through intraperitoneal injection of sodium pentobarbital/sodium diphenylhydantoin.

Macroscopic examination of the hair-bearing implantation areas was carried out, and samples were recovered following trichotomy. These samples were preserved in plastic containers with buffered formalin and dehydrated with alcohol, underwent xylol diaphanization, and infiltrated with paraffin using the Auto Technicon Tissue Processor™ from Leica Microsystem in Mannheim, Germany. The Thermo Scientific™ Histoplast Paraffin™ kit provided by Fisher Scientific in Waltham, MA, USA facilitated the cutting process.

2.7.1 Histological Analysis

Paraffin blocks containing the tissue samples were sliced to a thickness of 5 µm using the Leica microtome instrument. Then, the blocks were histologically analyzed using the hematoxylin-eosin (HE) and Masson's trichotomy (MT) staining techniques. The Leica DFC 295 camera and Leica DM750 optical microscope were employed to capture images. These images were then interpreted using the Lecia Microsystems 4.12.0 software provided by Leica Microsystems based in Mannheim, Germany.

The ethical approval and oversight for the study were conducted by the Biomedical Experimentation Animal Ethics Committee (CEAS) at the Universidad del Valle. The study adhered to the guidelines established by the "Animal Research: Reporting of In Vivo Experiments" (ARRIVE) guidelines [42]. Throughout the research, no intraoperative or postoperative complications, nor any instances of biomodel fatalities, were observed. The inclusion criteria solely considered factors like sex, age, and weight, while discontinuation criteria encompassed any situation that might impact the animals' well-being, including intraoperative or postoperative complications.

3. Results and Discussion

3.1. Characterization of ZnO-NPs

ZnO-NPs were synthesized according to previous methodologies [37]. The characterization of this component can be found in previous works [39].

3.2. GEO characterization

GC-MS performed the chemical composition of the GEO through the NIST library based on molecular weight and retention index. Table S1 summarizes the design of the main molecules found in the GEO. In this oil, 46 components were found, where the most prominent compounds were α-Zingiberene (28.5%), β-sesquiphellandrene (13.7%), α-curcumene (9.3%), β-Bisabolene (7.6%), trans-trans-α-Farnesene (5.6%), Camphene (5.3%), β-Felandrene (4.3%), sesquiterpene hydrocarbon (2.9%), according to previous research [43], mainly influenced by age, genetic composition, separation processes, and edaphic conditions.

3.3. FT-IR Spectroscopy

The analysis of the different functional groups present in the membranes was observed in Figure 1. In general, the characteristic bands of PCL and PLA were found at 2945, 1756, 1722, 1182, 1085 cm-1 attributed to the CH alkyl groups, the two bands corresponding to the vibrational modes of the ester-like C=O groups present in the polymeric-matrix, the asymmetric tension vibrational mode of the C-O-C group present within the aliphatic chain of the polymer and finally the asymmetric tension vibrational mode of the CO group. Except for F2, it was observed that the introduction of GEO or ZnO-NPs did not produce significant variations in the FTIR spectrum, probably due to the small amount of the different components within the formulation; therefore, the bands attributed to the polymeric matrix prevail in contrast to the vibrational modes present in the GEO or ZnO-NPs. However, substantial changes were noted in the intensity of the bands attributed to molecular interactions.

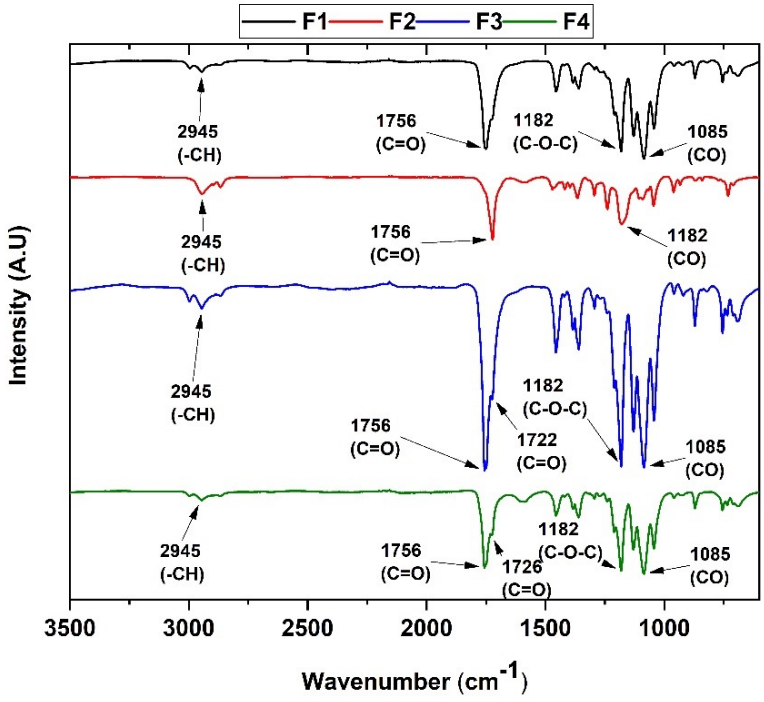

Figura 1. Espectro FT-IR de las membranas de PCL/PLA/ZnO-NPs/GEO. F1, 25%PCL/70%PLA; F2, 27%PCL/70%PLA/3%ZnO-NPs; F3, 20%PCL/70%PLA/10%GEO; F4, 17%PCL/70%PLA/3%ZnO-NPs/10%GEO.
Figure 1. FT-IR spectrum of PCL/PLA/ZnO-NPs/GEO membranes. F1, 25%PCL/70%PLA; F2, 27%PCL/70%PLA/3%ZnO-NPs; F3, 20%PCL/70%PLA/10%GEO; F4, 17%PCL/70%PLA/3%ZnO-NPs/10%GEO.

Consequently, the absence of additional vibrational modes implies that the interactions between the polymer matrix (PCL and PLA), the GEO, and the ZnO-NPs are mainly physical rather than chemical. On the other hand, two characteristic vibrational modes for the C=O groups present in the PLA and PCL polymeric matrix in F1, F3, and F4 were observed at 1756 and 1722 cm-1, respectively [44,45]. For F2, only the band at 1756 cm-1 was observed, which is related to the interaction between the C=O groups present in the polymeric matrix with the ZnO-NPs promoting the accumulation of lactide and acetaldehyde groups due to the degradation of the polymeric chain induced by ZnO-NPs [28]. Additionally, an increase in the intensity of the C-O-C vibrational mode at 1085 cm-1 was observed at F3, possibly due to the presence of GEO and the formation of hydrogen bonds with the polymers [46].

3.4. X-ray Diffraction

The characteristic peaks resulting from the interaction between the X-rays and the membranes are shown in Figure 2. For both PLA and PCL, their orthorhombic naturalization was observed due to the position of each characteristic peak. Concerning PLA, 2θ shifts at 14.7, 16.6, 19.0, and 22.1 were observed, which agree with previous investigations [47]. Additionally, 2θ changes to 21.3 and 23.6 for the PCL were observed, attributed to the (110) and (200) planes, respectively [48].

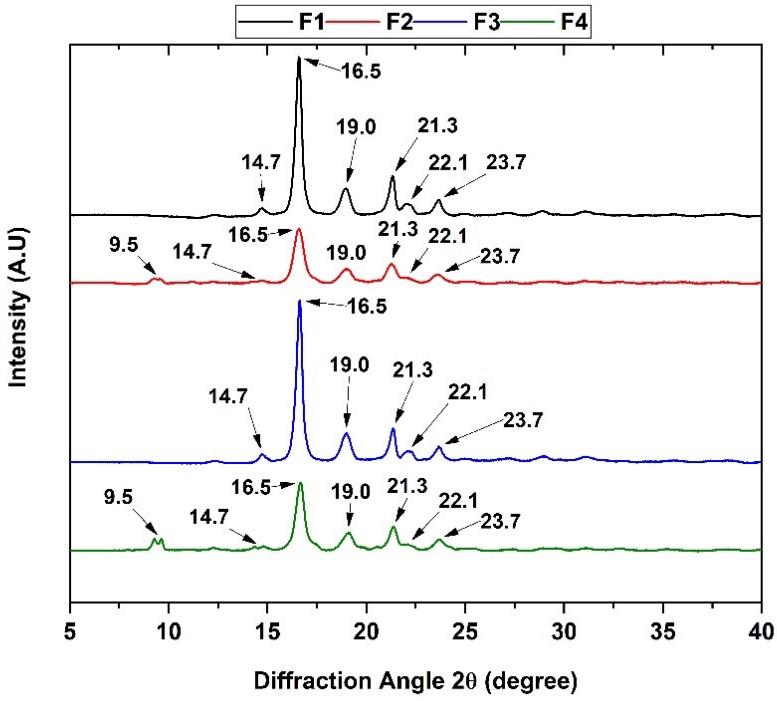

Figura 2. Análisis DRX de las membranas PCL/PLA/ZnO-NPs/GEO.
Figure 2. XRD analysis of PCL/PLA/ZnO-NPs/GEO membranes.

On the other hand, the diffractogram showed a decrease in crystallinity due to the addition of the ZnO-NPs and GEO compounds. The above is probably due to the reduction of intramolecular interactions along the polymeric chain between the C=O groups with the ZnO-NPs, causing the degradation of the polymeric matrix and inducing the appearance of new diffraction peaks as observed in the diffraction angle 2θ at 9° for the formulation F2 and F4 [49]. In addition, the addition of GEO induces a decrease in crystallinity, evidenced by the reduction of the intensity of the diffraction peaks, as observed in previous work with essential oils [6].

3.5. Thermal Analysis of PLA/PCL/GEO/ZnO-NPs.

The thermal degradation of the membranes as the temperature increases is shown in Figure 3. The thermograms show that, as the ZnO-NPs or GEO are incorporated, the thermal stability of the membranes decreases, probably due to the interaction between the ZnO-NPs with the C=O groups of the polymeric matrix, crosslinking the polymers, causing the formation of intramolecular spaces that decrease the strength of the bond and stability [50]. However, the introduction of GEO causes a not-so-significant gain of thermal stability probably due to the presence of thermostable molecules, which is consistent when comparing F2 with F3, but if it was observed with respect between F1 and F3, the loss of thermal stability is due to the little intermolecular interaction between PCL and PLA polymers with GEO, as it has been observed for similar works with other essential oils [51].

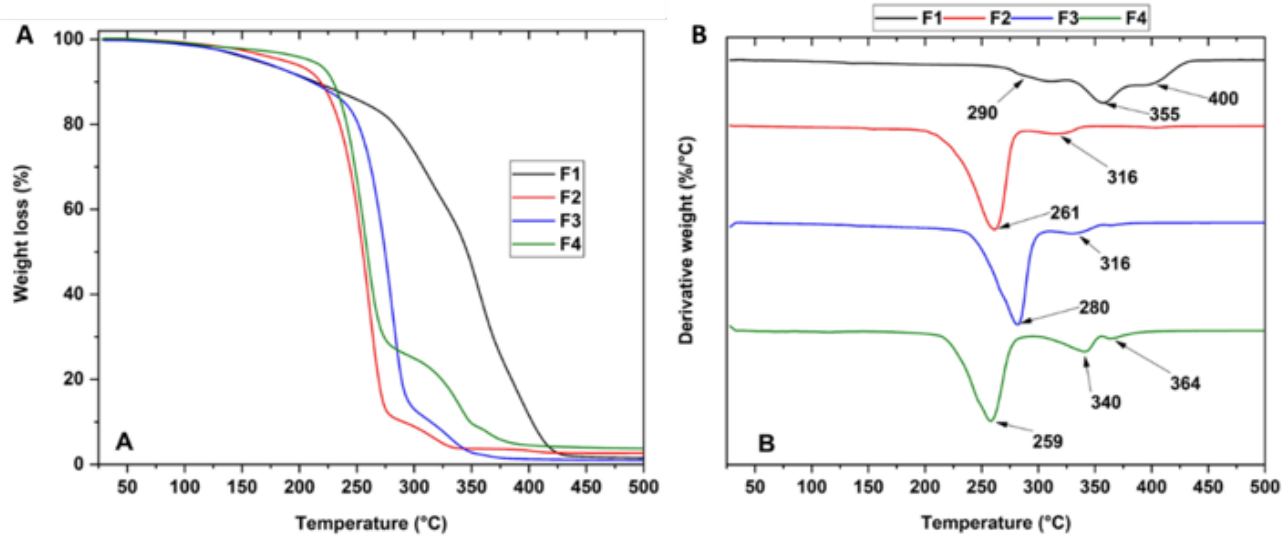

Figura 3. Análisis termogravimétrico de las membranas PCL/PLA/ZnO-NPs/GEO.
A) Termograma (TGA) y sus curvas derivadas (B) de las membranas F1, F2, F3 y F4.
Figure 3. Themogravimetric análisis of the PCL/PLA/ZnO-NPs/GEO membranes.
A) thermogram (TGA) and its derivate curves (B) of the membranes F1, F2, F3, and F4.

Figure 3A shows the thermogram corresponding to membranes F1, F2, F3, and F4. In this sense, three stages of degradation can be observed in the thermogram for F1. The first and second stages are between 265-323 and 326-383°C, respectively, associated with intramolecular incisions causing the formation of low molecular weight molecules such as lactides or cyclic oligomers [52]. The third stage of degradation is between 383-441°C, corresponding to the decomposition of the PCL induced by the insertion of the OH groups, causing the depolymerization of the polymeric matrix [13].

On the other hand, no significant differences are observed between the degradation temperatures of the formulations F2, F3, and F4, which contain amounts of ZnO-NPs or GEO. However, when comparing these formulations with F1, a decrease in the degradation temperature of approximately 31 °C is observed. The reduction in the degradation temperature probably occurs because the ZnO-NPs generate degradative processes, causing the formation of low molecular weight chains of PLA and PCL related to the transesterification processes and incisions of the carbon chain [29]. The latter induces the formation of additional voids by crosslinking the ZnO-NPs, and the C=O groups decrease the order promoted by the intramolecular bonds [53]. Additionally, the introduction of GEO decreases the thermal stability in contrast to F1, probably due to the interaction of GEO with the carbonyl groups of the polymeric matrix, causing the introduction of intramolecular spaces [54,55], consistent with previous research [6].

Differential scanning calorimetry (DSC) allows the determination of the thermal properties of the membranes as the temperature increases, as shown in Figure 4. The thermogram shows the glass transition temperature (Tg) and the melting temperatures of the polymeric matrix for PCL (Tm1) and PLA (Tm2 and Tm3). All data are summarized in Table 2.

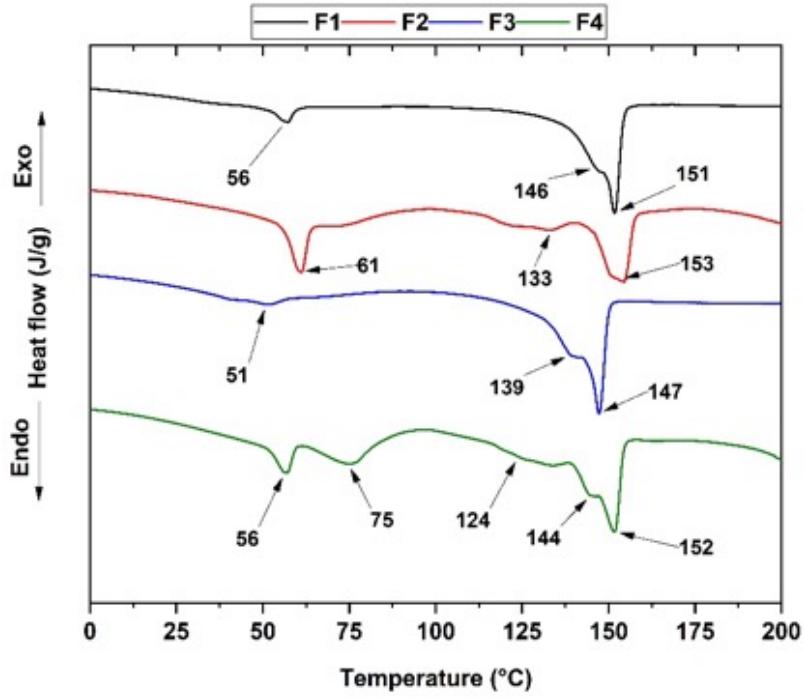

Figura 4. Curvas DSC de las membranas PCL/PLA/ZnO-NPs/GEO.
Figure 4. DSC curves of the PCL/PLA/ZnO-NPs/GEO membranes.

The calculation of the crystallinity for the different membranes is very complex because the Tg for PLA (60°C) is very close to the melting temperature for PCL (Tm1); moreover, in all formulations, the enthalpy of crystallization is not present. Thermal characterization indicates no favoring of the crystalline forms that can occur for PLA. It has been observed in these composites that two different crystalline structures can be found for PLA because they present the same cross-linking energy shown in previous works [56]. However, by action by ZnO-NPs or essential oils, they can favor the adoption of the α-form attributed to the PLA. As the temperature increases, the packing tends to the β-form (orthorhombic or trigonal) or the α-form (pseudo-orthorhombic, pseudo-hexagonal, and orthorhombic) probably because the introduction of ZnO-NPs generates nucleation sites which increase the melting points as it degrades the polymeric matrix as observed for F4 [57,58].

Tabla 2. Propiedades térmicas de las membranas PCL/PLA/ZnO-NPs/GEO.
Table 2. Thermal properties of the PCL/PLA/ZnO-NPs/GEO membranes.

	T_g (°C)	T_{m1} (°C)	T_{m2} (°C)	T_{m3} (°C)
F1	55	56	146	151
F2	58	61	133	153
F3	56	51	139	147
F4	54	56	144	152

On the other hand, the membranes do not present the crystallization temperature for PLA, which is taken as the exothermic peak present in the formulation. This is probably due to the incompatibility of the polymeric matrix hindering the macromolecular interaction between the carbonyl or hydroxyl groups, generating the instability of the crystalline structure [59,60].

3.6 Scanning Electron Microscopy (SEM) of PLA/PCL/GEO/ZnO-NPs membranes.

The morphological microstructure of the PCL/PLA/GEO/ZnO-NP membranes can be seen in Figure 5. Except for F1, the membranes show a porous microstructure, which may facilitate the interaction with other components due to the low macromolecular interaction between PLA and PCL polymers [61]. Moreover, the introduction of ZnO-NPs or GEO prevents this interaction probably because these components interact with the C=O groups through hydrogen bonds as in the case of GEO or incision points caused by the interaction between this functional group and the ZnO-NPs as mentioned above [53].

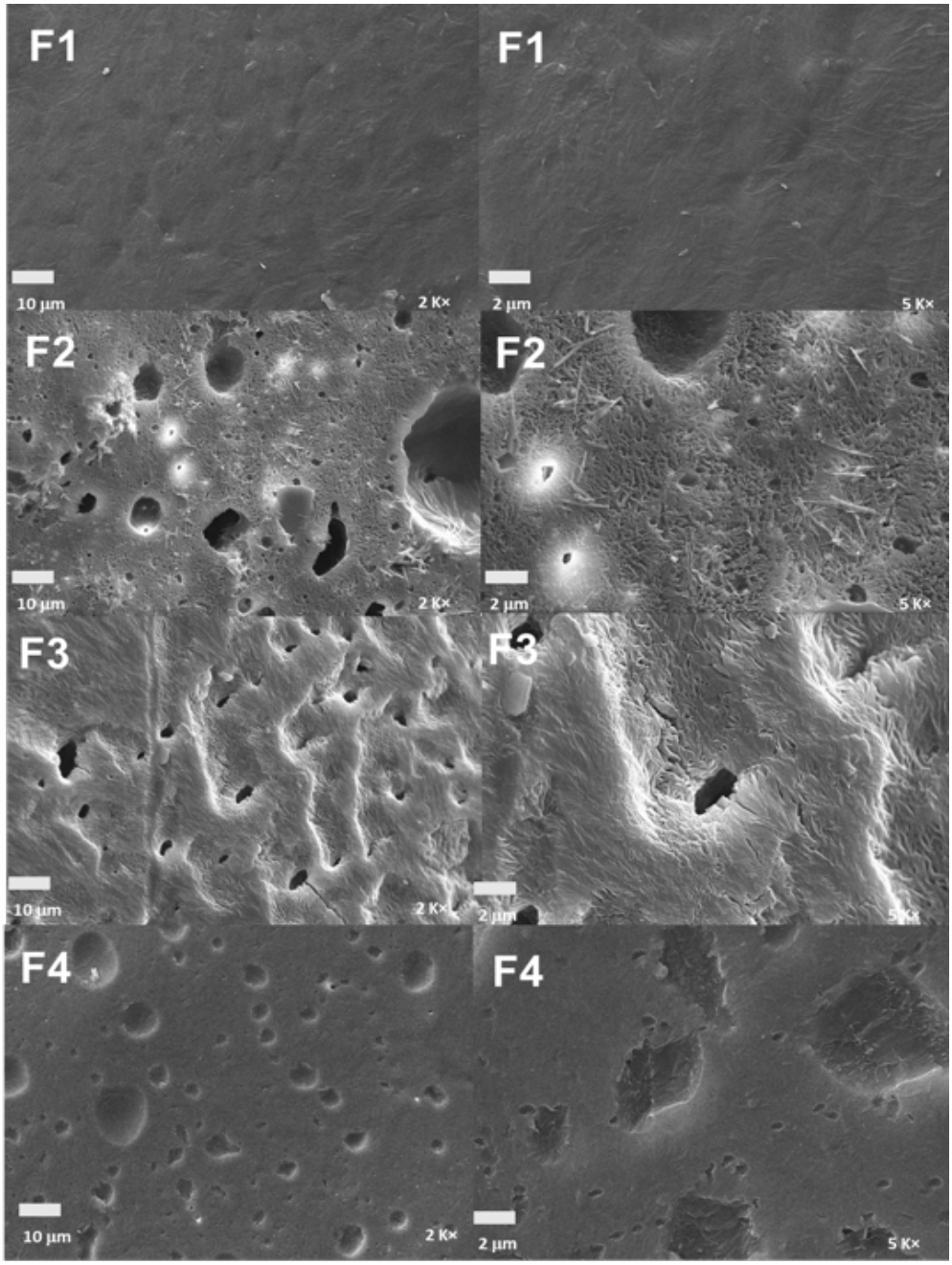

Figura 5. Morfología de las membranas PCL/PLA/GEO/ZnO-NPs. F1, 25%PCL/70%PLA a 2000 y 5000×; F2, 27%PCL/70%PLA/3%ZnO-NPs a 2000 y 5000×; F3, 20%PCL/70%PLA/10%GEO a 2000 y 5000×; F4, 17%PCL/70%PLA/3%ZnO-NPs/10%GEO a 2000 y 5000×.

Figure 5. Morphology of membranes PCL/PLA/GEO/ZnO-NPs membranes. F1, 25%PCL/70%PLA at 2000 and 5000×; F2, 27%PCL/70%PLA/3%ZnO-NPs at 2000 and 5000×; F3, 20%PCL/70%PLA/10%GEO at 2000 and 5000×; F4, 17%PCL/70%PLA/3%ZnO-NPs/10%GEO at 2000 and 5000×.

On the other hand, the voids on the membrane F2 are probably due to inadequate interfacial interactions between the ZnO-NPs and the polymeric matrix, causing new nucleation sites due to the reduction of elasticity of the PLA chains [62]. Additionally, sample F3 presents the same morphology as F2 because, during the membrane formation process, the volatile components present in GEO partially evaporate when the mixture is subjected to 40°C in a preheated oven, generating the dispersion of the polymeric matrix causing the formation of voids [63]. Finally, the F4 formulation shows a more compact morphology with fewer irregularities on the surface, probably because both ZnO-Nps and GEO act synergically, facilitating the dispersion of the components on the polymeric matrix [64].

3.7. In Vivo Biocompatibility Tests of the PLA/PCL/GEO/ZnO-NPs membranes

In Figure 6, we can observe the implantation site on the dorsal area of the biomodels. Notably, there was a complete and healthy recovery with hair regrowth, and no signs of purulent exudate were detected in any of the biomodels. Subsequent staining analyses revealed that the lesions resulting from the material implantation had healed without an aggressive immune response. Furthermore, collagen fiber capsules surrounding the material suggest the healing process progresses. These collagen fibers secure the material without inciting an adverse immune reaction, which is crucial for stability until removal for histological analysis.

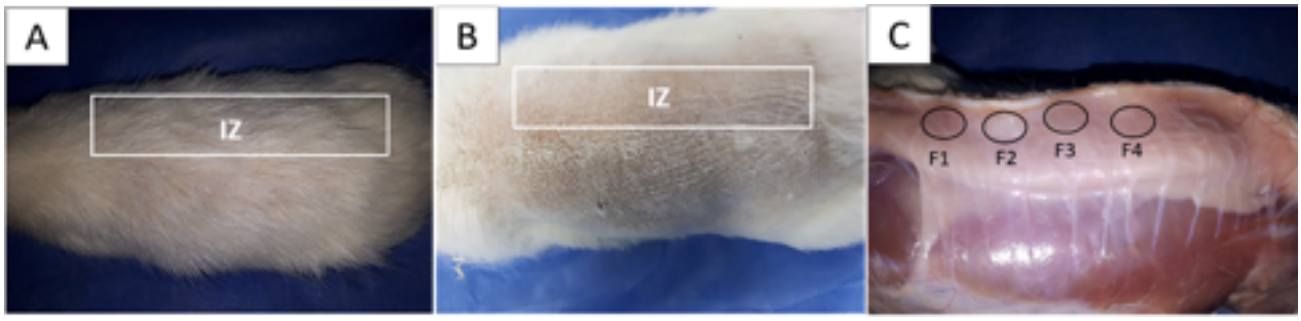

Figura 6. Aspecto microscópico de la zona implantada. A: recrecimiento del pelo. B: Imagen con tricotomía. C: Superficie interna de la piel. Círculo F1: Zona de implantación formulación F1. Círculo F2: Zona de implantación formulación F2. Círculo F3: Zona de implantación formulación F3. Círculo F4: Zona de implantación formulación F4.

Figure 6. Microscopic aspect of the implanted area. A: Hair regrowth. B: image with trichotomy. C: Internal surface of the skin. F1 circle: F1 formulation im-plantation zone. Circle F2: Implantation zone formulation F2. Circle F3: Implantation zone formulation F3. Circle F4: Implantation zone formulation F4.

3.7.1 Biocompatibility of formulation F1

The histological image corresponding to the implantations of the F1 material indicates that 60 days after the intervention, the film composed of PCL 30/ PLA% 70% shows little evidence of resorption or degradation; in Figure 7A, the oval corresponds to the implantation zone. It is possible to observe by Masson's tri-chrome staining a fragment of the material surrounded by a thick capsule with abundant collagen type I blue fibers (Figure 7B). At a magnification of 100×, large inflammatory cells also form the fibrous capsule (Figure 7C).

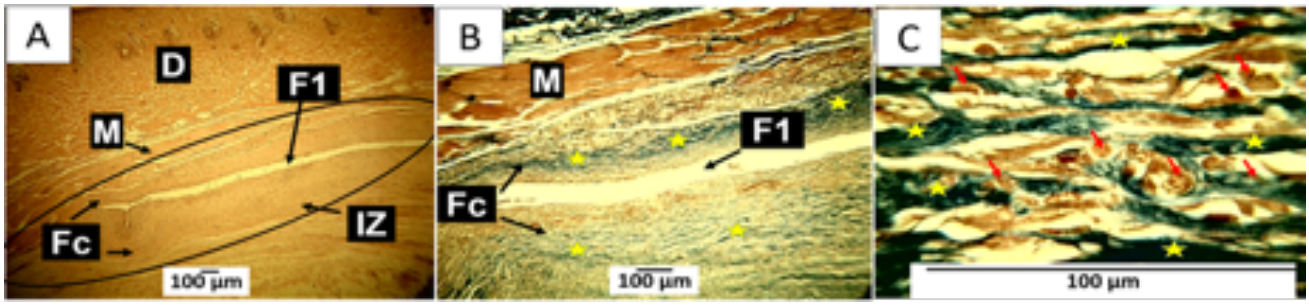

Figura 7. Implantación subdérmica del material F1 a los 60 días. A: Imagen 4×. Técnica HE. B: Imagen a 10× técnica TM. C: Imagen a 100× técnica TM. D: Dermis; M: músculo; IZ: zona de implantación; Fc: casquete fibroso. F1: Lámina F1. Estrellas amarillas: fibras de colágeno de tipo I. Flechas rojas: células inflamatorias.

Figure 7. Subdermal implantation of F1 material at 60 days. A: 4× image. HE technique. B: Image at 10× TM technique. C: Image at 100× TM technique. D: Dermis; M: muscle; IZ: implantation zone; Fc: fibrous cap. F1: F1 film. Yellow stars: type I collagen fibers. Red arrows: inflammatory cells.

The F2 formulation was modified compared to F1 by decreasing the percentage of PCL to 27% and adding 3% of ZnO. When the histological images are reviewed 60 days after implantation, an essential change in the biological behavior of the samples is observed. In Figure 8A, the implantation zone is surrounded by a fibrous capsule in a similar way to that found for F1, but with a notable difference in the thickness of the capsule. The presence of a material of reticular appearance, compatible with connective tissue, is also observed in the area where the experimental material was deposited (green stars, Figure 8A).

Figure 8B corresponds to a sample that was oriented horizontally to obtain longitudinal sections of the sample parallel to the dermis; it can be observed that the reticular tissue forms the implantation zone already mentioned, formed by fibers with negative staining for MT (purple arrows in the zone demarcated by the black circle); in some of the demarcated areas there is also intense staining for MT, compatible with type I collagen (blue regions); at a magnification of 40× it is observed how the reticular structure is separating small portions of the sample with the presence of inflammatory cells. The fibers also demarcate areas without staining where the experimental material seems to have been replaced by type I collagen (Figure 8C).

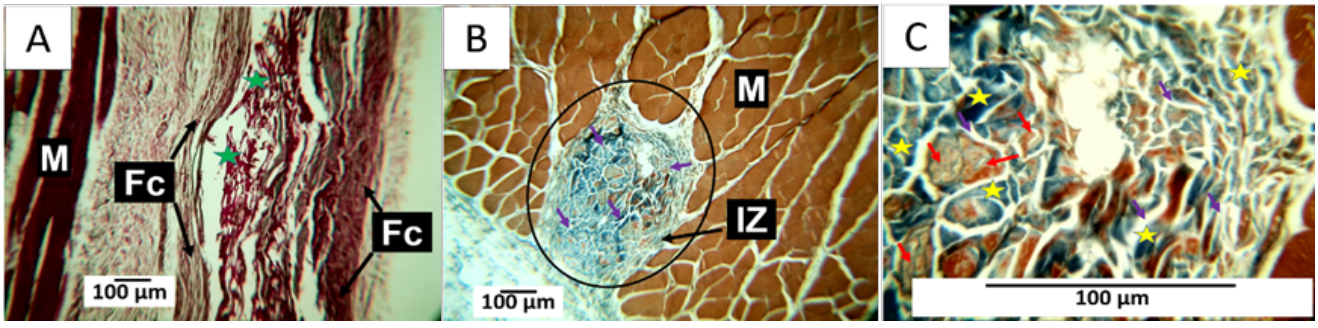

Figura 8. Implantación subdérmica del material F2 a los 60 días. A: Imagen 10×. Técnica HE. B: Imagen a 10× técnica MT. C: Imagen a 40× técnica MT. M: músculo; Fc: capa fibrosa. Estrellas verdes. Tejido conjuntivo. Flechas moradas. Fibras de tejido conjuntivo nocivas para la MT, Estrellas amarillas: colágeno tipo I. Flechas rojas: células inflamatorias.
Figure 8. Subdermal implantation of the F2 material at 60 days. A: 10× image. HE technique. B: Image at 10× MT technique. C: Image at 40× MT technique. M: muscle; Fc: fibrous cap. Green stars. Connective tissue. Purple arrows. Connective tissue fibers are harmful to MT. Yellow stars are type I collagen—red arrows: inflammatory cells.

3.7.3 Biocompatibility of formulation F3

The F3 formulation also presents an essential modification concerning the F1 formulation; the PCL was reduced to 20%, and 10% of GEO was incorporated. The histological images of the implantation zone showed that at 60 days, connective tissue and inflammatory infiltrate are present, surrounded by a fibrous capsule (Figure 9A). Figure 9B corresponds to a longitudinal section employing staining with MT; the presence of abundant collagen fibers was evidenced (Figure 9B), while the comparison with F2 formulation exhibits the presence of more significant collagen presence with a more homogeneous appearance.

The longitudinal section shows how the implantation zone is occupied by a septum of type I collagen fibers that subdivide the site into smaller areas, each occupied by smaller fibers surrounding small portions of the experimental material with inflammatory cells (Figure 9C).

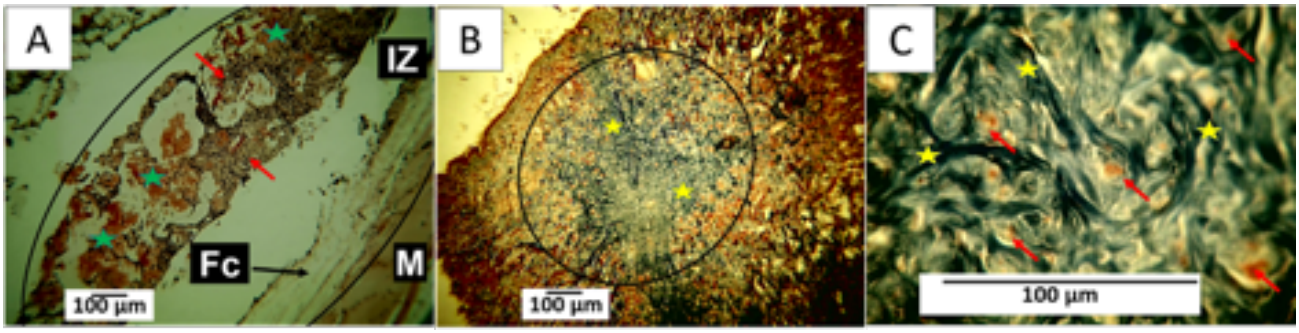

Figura 9. Implantación subdérmica de material F3 a los 60 días. A: Imagen 10×. Técnica HE. B: Imagen a 10× técnica MT. C: Imagen a 40× técnica MT; IZ: zona de implantación; Fc: casquete fibroso. Estrellas verdes: tejido conjuntivo; flechas rojas: células inflamatorias; estrellas amarillas: colágeno tipo I.

Figure 9. Subdermal implantation of F3 material at 60 days. A: 10× image. HE technique. B: Image at 10× MT technique. C: Image at 40× MT technique; IZ: implantation zone; Fc: fibrous cap. Green stars: connective tissue; red arrows: inflammatory cells; yellow stars: type I collagen.

3.7.4 Biocompatibility of formulation F4

The results of implantation of formulation 4 show almost complete resorption of the material; in Figure 10A, the presence of some fragments of the material is observed; at a magnification of 10× and through MT staining, the implantation area is occupied by connective tissue rich in type I collagen fibers, with the presence of small fragments of the material; at higher magnification (100×), the presence of abundant collagen fibers is observed, with very little presence of the material.

The results of this formulation were different from those observed for the other formulations, as there was almost complete resorption of the material with the absence of the fibrous capsule, which may be due to the modification of the formulation, which about F1 presents a decrease in the percentage of PCL, with the addition of 3% of ZnO and 10% of GEO.

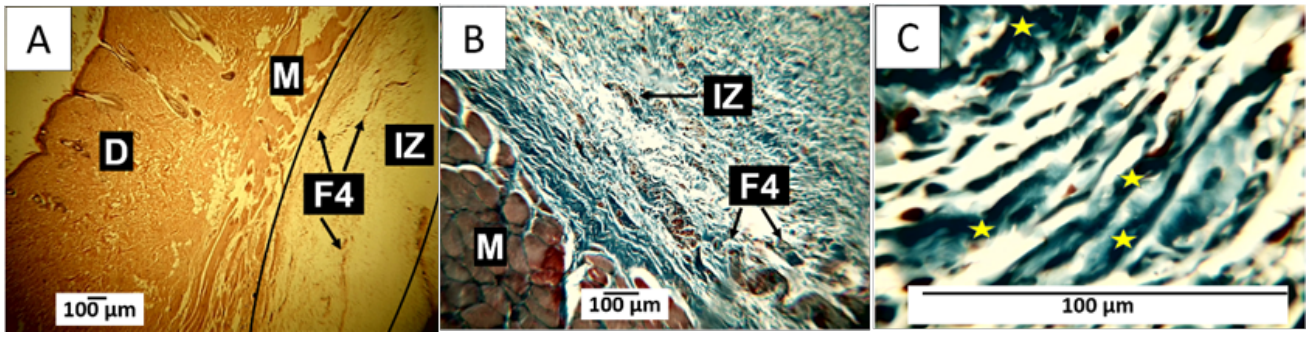

Figura 10. Implantación subdérmica de material F4 a los 60 días. A: Imagen 4x. Técnica HE. B: Imagen a 10× técnica MT. C: Imagen a 100× técnica MT; D: Dermis; M: Músculo: Dermis; M: Músculo; IZ: Zona de implantación; F4: Material implantado; Estrellas amarillas: Colágeno tipo I.

Figure 10. Subdermal implantation of F4 material at 60 days. A: 4x image. HE technique. B: Image at 10× MT technique. C: Image at 100× MT technique; D: Dermis; M: Muscle: Dermis; M: Muscle; IZ: Implantation zone; F4: Implanted material; Yellow stars: Collagen type I.

The histological results for the four materials differed, which can be explained by the composition differences. All formulations were mainly composed of PCL and PLA with some modifications, incorporating ZnO-NPs and GEO. The implantation of material in living tissue incites a biological response whose severity is determined by the material-tissue interaction and will be influenced by different factors such as the implantation site and physical, chemical, and biological properties of the material [65], especially by the degradation kinetics and

degradation products [66]. The interaction process between the host immune system and the biomaterial may lead to product encapsulation to control the presence and limit damage [67].

PLA and PCL have been widely employed in biomedical applications due to their biocompatibility, degradability, and mechanical properties [67]. The combination of PLA and PCL has been the subject of numerous studies because the combination allows mechanical properties and resorption rate adjustment. After all, PCL increases PLA crystallization [68].

This work showed that the F1 formulation composed of PCL 30/ PLA% 70% at 60 days presented little evidence of resorption and encouraged an inflammatory response type foreign body reaction with a very thick fibrous encapsulation (Figure 7A). However, when decreasing the percentage of PCL to 27% and increasing 3% of ZnO-Nps (formulation F2), the foreign body reaction still exists, but the fibrous capsule decreases in size. Connective tissue with a reticular appearance composed of collagen fibers (Type I) was also observed.

The effect of decreasing the percentage of PCL in formulation two possibly decreased the resorption rate of the product, which was reflected histologically in the resorption/partial degradation of the product and replacement by connective tissue, as can be seen in Figure 8, where a change in the behavior of the material is observed, with the presence of connective tissue due to the incorporation of ZnO-Nps. It has been reported that ZnO-Nps acts on cells, promoting adhesion, growth, cell differentiation, and angiogenesis [69], which would help explain this slight variation between formulations 1 and 2.

Like the other two formulations, samples developed from formulation F3 showed a foreign body reaction with fibrous encapsulation. No ZnO-Nps was incorporated in this case, but 10% GEO was included instead. The histological image of formulation F3 corresponds to a sample in an evident degradation process with inflammatory cells, which the incorporation of GEO may have stimulated. This essential oil has been reported to have some biomedical properties, such as being a healing stimulant and anti-inflammatory in induced skin lesions [70]. There are some notable differences between the F2 and F3 formulations. In the histological results of the F2 sample, a healing process is observed in which there is resorption of the material and engulfment of particles by a cross-linking of type I collagen fibers (Figure 8). In contrast, in F3 formulation, the resorption process seems to be more advanced, and there is a more significant presence of cells. A more homogeneous connective tissue occupies the implantation zone, made up of type I collagen fibers, and where the fragments of the material are no longer so evident, giving the impression that the GEO accelerated the scarring process through greater cellular participation (Figure 9).

By incorporating ZnO-Nps and GEO into PCL/PLA (Figure 10), a synergistic effect appears to occur, leading to rapid resorption/degradation of the PCL/PLA matrix, with only tiny fragments of the films being evident after 60 days, and their replacement by connective scar tissue without the formation of a fibrous capsule.

4. Conclusions

In this research, we synthesized four membranes composed of PLA/PCL/GEO/ZnO-NPs, which displayed enhanced thermal stability compared to their components. The incorporation of ZnO-NPs was confirmed through various characterization techniques such as FTIR, XRD, TGA, and DSC. In FTIR analysis, we observed a reduction in the band at 1722 cm-1 associated with the C=O groups in PCL, indicating the predominant interaction of ZnO-NPs with this functional group as well as the increase of the C-O-C band due to the formation of hydrogen bonds between the GEO and the carbonyl groups. Furthermore, we noticed a decrease in thermal properties and crystallinity as the concentration of ZnO-NPs decreases by forming intermolecular spaces due to the interaction of the carbonyl groups of the polymeric matrix with the ZnO-NPs or GEO. SEM analysis revealed that adding GEO or ZnO-NPs created a porous morphology in the composites due to polymer incompatibility. However, it was revealed that in the F4 formulation, GEO and ZnO-NPs synergistically led to homogeneous surfaces.

Additionally, the PLA/PCL/GEO/ZnO-NPs membranes exhibited preliminary biocompatibility, undergoing degradation and resorption, along with a rapid healing process that resulted in the complete restoration of tissue architecture. Notably, there was no sign of an aggressive immune response. During the resolution process, the material fragmented and was absorbed by inflammatory cells, stimulating the proliferation of collagen fibers, blood vessels, and cells, thus continuing the material resorption process. On the other hand, the results for la formulation F4 differed from those observed for the different formulations as there was almost complete resorption of the material with the absence of the fibrous capsule, which may be due to the modification of the formulation. These results underscore the significance and potential impact of ZnO-NP-based scaffolds in soft tissue regeneration.

5. References

1. Mahmoudi, N.; Eslahi, N.; Mehdipour, A.; Mohammadi, M.; Akbari, M.; Samadikuchaksaraei, A.; Simchi, A. Temporary skin grafts based on hybrid graphene oxide natural biopolymer nanofibers as adequate wound healing substitutes: pre-clinical and pathological studies in animal models. J. Mater. Sci. Mater. Med. 2017, 28, 1–13.

2. Bacakova, L.; Pajorova, J.; Bacakova, M.; Skogberg, A.; Kallio, P.; Kolarova, K.; Svorcik, V. Versa-tile application of nanocellulose: From industry to skin tissue engineering and wound healing. Nano-materials 2019, 9, 164.

3. Zhang, Y.; Poon, K.; Masonsong, G.S.P.; Ramaswamy, Y.; Singh, G. Sustainable Nanomaterials for Biomedical Applications. Pharmaceutics 2023, 15, 922.

4. O'Brien, F.J. Biomaterials & scaffolds for tissue engineering. Mater. Today 2011, 14, 88–95, doi:10.1016/S1369-7021(11)70058-X.

5. Arif, U.; Haider, S.; Haider, A.; Khan, N.; Alghyamah, A.A.; Jamila, N.; Khan, M.I.; Almasry, W.A.; Kang, I.-K. Biocompatible polymers and their potential biomedical applications: A review. Curr. Pharm. Des. 2019, 25, 3608–3619.

6. Grande-Tovar, C.D.; Castro, J.I.; Valencia Llano, C.H.; Tenorio, D.L.; Saavedra, M.; Zapata, P.A.; Chaur, M.N. Polycaprolactone (PCL)-Polylactic Acid (PLA)-Glycerol (Gly) Composites Incorporated with Zinc Oxide Nanoparticles (ZnO-NPs) and Tea Tree Essential Oil (TTEO) for Tissue Engineering Applications. Pharmaceutics 2022, 15, 43.

7. Tovar, C.D.G.; Castro, J.I.; Valencia, C.H.; Porras, D.P.N.; Hernandez, J.H.M.; Valencia, M.E.; Ve-lásquez, J.D.; Chaur, M.N. Preparation of chitosan/poly(Vinyl alcohol) nanocomposite films incorporated with oxidized carbon nano-onions (multi-layer fullerenes) for tissue-engineering applications. Biomolecules 2019, 9, doi:10.3390/biom9110684.

8. Martin, I.; Wendt, D.; Heberer, M. The role of bioreactors in tissue engineering. TRENDS Biotechnol. 2004, 22, 80–86.

9. Deb, P.; Deoghare, A.B.; Borah, A.; Barua, E.; Das Lala, S. Scaffold Development Using Biomateri-als: A Review. Mater. Today Proc. 2018, 5, 12909–12919, doi:10.1016/j.matpr.2018.02.276.

10. Avérous, L.; Pollet, E. Environmental silicate nano-biocomposites; Springer, 2012; Vol. 1;.

11. Santoro, M.; Shah, S.R.; Walker, J.L.; Mikos, A.G. Poly (lactic acid) nanofibrous scaffolds for tissue engineering. Adv. Drug Deliv. Rev. 2016, 107, 206–212.

12. Fortelny, I.; Ujcic, A.; Fambri, L.; Slouf, M. Phase structure, compatibility, and toughness of PLA/PCL blends: A review. Front. Mater. 2019, 6, 206.

13. Mina Hernandez, J.H. Effect of the incorporation of polycaprolactone (Pcl) on the retrogradation of binary blends with cassava thermoplastic starch (tps). Polymers (Basel). 2021, 13, 1–19, doi:10.3390/polym13010038.

14. Fambri, L.; Migliaresi, C. Crystallization and thermal properties. Poly (Lactic Acid) Synth. Struct. Prop. Process. Appl. End Life 2022, 135–151.

15. Standau, T.; Zhao, C.; Murillo Castellón, S.; Bonten, C.; Altstädt, V. Chemical modification and foam processing of polylactide (PLA). Polymers (Basel). 2019, 11, 306.

16. Vasile, C.; Râpă, M.; Ştefan, M.; Stan, M.; Macavei, S.; Darie-Niţă, R.N.; Barbu-Tudoran, L.; Vodnar, D.C.; Popa, E.E.; Ştefan, R. New PLA/ZnO: Cu/Ag bionanocomposites for food packaging. Express Polym. Lett. 2017, 11.

17. Spoială, A.; Ilie, C.-I.; Truşcă, R.-D.; Oprea, O.-C.; Surdu, V.-A.; Vasile, B. Ștefan; Ficai, A.; Ficai, D.; Andronescu, E.; Dițu, L.-M. Zinc oxide nanoparticles for water purification. Materials (Basel). 2021, 14, 4747.

18. Alharthi, M.N.; Ismail, I.; Bellucci, S.; Khdary, N.H.; Abdel Salam, M. Biosynthesis micro-wave-assisted of zinc oxide nanoparticles with ziziphus jujuba leaves extract: Characterization and photocatalytic application. Nanomaterials 2021, 11, 1682.

19. Vasile, O.-R.; Andronescu, E.; Ghitulica, C.; Vasile, B.S.; Oprea, O.; Vasile, E.; Trusca, R. Synthesis and characterization of nanostructured zinc oxide particles synthesized by the pyrosol method. J. Na-noparticle Res. 2012, 14, 1–13.

20. Serb, M.-D.; Mueller, P.; Trusca, R.; Oprea, O.; Dumitru, F. Study of thermal decomposition of a zinc (ii) monomethyl terephthalate complex, [zn (ch3o-co-c6h4coo)(2)(oh2)(3)] center dot 2h (2) o. J. Therm. Anal. Calorim. 2015, 121, 691–695.

21. Motelica, L.; Vasile, B.-S.; Ficai, A.; Surdu, A.-V.; Ficai, D.; Oprea, O.-C.; Andronescu, E.; Jinga, D.C.; Holban, A.M. Influence of the alcohols on the zno synthesis and its properties: The photocata-lytic and antimicrobial activities. Pharmaceutics 2022, 14, 2842.

22. Rojas, K.; Canales, D.; Amigo, N.; Montoille, L.; Cament, A.; Rivas, L.M.; Gil-Castell, O.; Reyes, P.; Ulloa, M.T.; Ribes-Greus, A. Effective antimicrobial materials based on low-density polyethylene (LDPE) with zinc oxide (ZnO) nanoparticles. Compos. Part B Eng. 2019, 172, 173–178.

23. Sirelkhatim, A.; Mahmud, S.; Seeni, A.; Kaus, N.H.M.; Ann, L.C.; Bakhori, S.K.M.; Hasan, H.; Mo-hamad, D. Review on zinc oxide nanoparticles: antibacterial activity and toxicity mechanism. Nano-micro Lett. 2015, 7, 219–242.

24. Abou Elmaaty, T.M.; Mandour, B.A. ZnO and TiO2 nanoparticles as textile protecting agents against UV radiation: A review. Asian J. Chem. Sci 2018, 4, 1–14.

25. Kim, I.; Viswanathan, K.; Kasi, G.; Thanakkasaranee, S.; Sadeghi, K.; Seo, J. ZnO nanostructures in active antibacterial food packaging: preparation methods, antimicrobial mechanisms, safety issues, future prospects, and challenges. Food Rev. Int. 2022, 38, 537–565.

26. Roeinfard, M.; Bahari, A. Nanostructural characterization of the Fe3O4/ZnO magnetic nanocomposite as an application in medicine. J. Supercond. Nov. Magn. 2017, 30, 3541–3548.

27. Shankar, S.; Wang, L.-F.; Rhim, J.-W. Incorporation of zinc oxide nanoparticles improved the me-chanical, water vapor barrier, UV-light barrier, and antibacterial properties of PLA-based nanocompo-site films. Mater. Sci. Eng. C 2018, 93, 289–298.

28. Marra, A.; Rollo, G.; Cimmino, S.; Silvestre, C. Assessment on the effects of ZnO and Coated ZnO particles on iPP and PLA properties for application in food packaging. Coatings 2017, 7, 29.

29. Murariu, M.; Doumbia, A.; Bonnaud, L.; Dechief, A.; Paint, Y.; Ferreira, M.; Campagne, C.; Devaux, E.; Dubois, P. High-performance polylactide/ZnO nanocomposites designed for films and fibers with special end-use properties. Biomacromolecules 2011, 12, 1762–1771.

30. Pantani, R.; Gorrasi, G.; Vigliotta, G.; Murariu, M.; Dubois, P. PLA-ZnO nanocomposite films: Water vapor barrier properties and specific end-use characteristics. Eur. Polym. J. 2013, 49, 3471–3482.

31. Paidari, S.; Zamindar, N.; Tahergorabi, R.; Kargar, M.; Ezzati, S.; Shirani, N.; Musavi, S.H. Edible coating and films as promising packaging: a mini review. J. Food Meas. Charact. 2021, 15, 4205–4214.

32. Singh, G.; Maurya, S.; Catalan, C.; De Lampasona, M.P. Studies on essential oils, Part 42: chemical, antifungal, antioxidant and sprout suppressant studies on ginger essential oil and its oleoresin. Flavour Fragr. J. 2005, 20, 1–6.

33. Li, X.; Tu, Z.-C.; Sha, X.-M.; Ye, Y.-H.; Li, Z.-Y. Flavor, antimicrobial activity and physical proper-ties of gelatin film incorporated with of ginger essential oil. J. Food Sci. Technol. 2022, 1–10.

34. Bonilla, J.; Poloni, T.; Lourenço, R. V; Sobral, P.J.A. Antioxidant potential of eugenol and ginger essential oils with gelatin/chitosan films. Food Biosci 23: 107–114 2018.

35. Souza, V.G.L.; Pires, J.R.A.; Rodrigues, C.; Rodrigues, P.F.; Lopes, A.; Silva, R.J.; Caldeira, J.; Du-arte, M.P.; Fernandes, F.B.; Coelhoso, I.M. Physical and morphological characterization of chi-tosan/montmorillonite films incorporated with ginger essential oil. Coatings 2019, 9, 700.

36. Castro, J.I.; Valencia-Llano, C.H.; Valencia Zapata, M.E.; Restrepo, Y.J.; Mina Hernandez, J.H.; Na-via-Porras, D.P.; Valencia, Y.; Valencia, C.; Grande-Tovar, C.D. Chitosan/Polyvinyl Alcohol/Tea Tree Essential Oil Composite Films for Biomedical Applications. Polymers (Basel). 2021, 13, 3753.

37. Becheri, A.; Dürr, M.; Lo Nostro, P.; Baglioni, P. Synthesis and characterization of zinc oxide nanoparticles: application to textiles as UV-absorbers. J. Nanoparticle Res. 2008, 10, 679–689.

38. Yañez, D.; Guerrero, S.; Lieberwirth, I.; Ulloa, M.T.; Gomez, T.; Rabagliati, F.M.; Zapata, P.A. Photocatalytic inhibition of bacteria by TiO2 nanotubes-doped polyethylene composites. Appl. Catal. A Gen. 2015, 489, 255–261.

39. Grande-Tovar, C.D.; Castro, J.I.; Valencia Llano, C.H.; Tenorio, D.L.; Saavedra, M.; Zapata, P.A.; Chaur, M.N. Polycaprolactone (PCL)-Polylactic acid (PLA)-Glycerol (Gly) Composites Incorporated with Zinc Oxide Nanoparticles (ZnO-NPs) and Tea Tree Essential Oil (TTEO) for Tissue Engineering Applications. Pharmaceutics 2023, 15, 43.

40. De Jong, W.H.; Carraway, J.W.; Geertsma, R.E. In vivo and in vitro testing for the biological safety evaluation of biomaterials and medical devices. In Biocompatibility and Performance of Medical De-vices; Elsevier, 2020; pp. 123–166.

41. AEN/CTN Evaluación biológica de los productos sanitarios Parte: Parte 6: Ensayos relativos a los efectos locales después de la implantación; 1995; Vol. 51;.

42. Du Sert, N.P.; Hurst, V.; Ahluwalia, A.; Alam, S.; Avey, M.T.; Baker, M.; Browne, W.J.; Clark, A.; Cuthill, I.C.; Dirnagl, U.; et al. The arrive guidelines 2.0: Updated guidelines for reporting animal re-search. PLoS Biol. 2020, 18, 1–12, doi:10.1371/journal.pbio.3000410.

43. Raina, V.K.; Kumar, A.; Aggarwal, K.K. Essential oil composition of ginger (Zingiber officinale Roscoe) rhizomes from different place in India. J. Essent. Oil Bear. Plants 2005, 8, 187–191.

44. Chieng, B.W.; Ibrahim, N.A.; Wan Yunus, W.M.Z.; Hussein, M.Z. Poly (lactic acid)/poly (ethylene glycol) polymer nanocomposites: Effects of graphene nanoplatelets. Polymers (Basel). 2013, 6, 93–104.

45. Visan, A.I.; Popescu-Pelin, G.; Gherasim, O.; Mihailescu, A.; Socol, M.; Zgura, I.; Chiritoiu, M.; Elena Sima, L.; Antohe, F.; Ivan, L. Long-term evaluation of dip-coated pcl-blend-peg coatings in simulated conditions. Polymers (Basel). 2020, 12, 717.

46. Pardini, F.; Iregui, Á.; Faccia, P.; Amalvy, J.; González, A.; Irusta, L. Development and characteriza-tion of electrosprayed microcaspules of poly ε-caprolactone with citronella oil for mosquito-repellent application. Int. J. Polym. Anal. Charact. 2021, 26, 497–516, doi:10.1080/1023666X.2021.1916726.

47. Kaczmarek, H.; Nowicki, M.; Vuković-Kwiatkowska, I.; Nowakowska, S. Crosslinked blends of poly (lactic acid) and polyacrylates: AFM, DSC and XRD studies. J. Polym. Res. 2013, 20, 1–12.

48. Ocelić, V.; Vilko, B.; Dajana, M.; Grgić, K.; Ivančić, A. Biodegradable Polymer Blends Based on Thermoplastic Starch. J. Polym. Environ. 2020, 29 (2), 492–508, doi:10.1007/s10924-020-01874-w.

49. Jamnongkan, T.; Jaroensuk, O.; Khankhuean, A.; Laobuthee, A.; Srisawat, N.; Pangon, A.; Mongkholrattanasit, R.; Phuengphai, P.; Wattanakornsiri, A.; Huang, C.-F. A Comprehensive Evalua-tion of Mechanical, Thermal, and Antibacterial Properties of PLA/ZnO Nanoflower Biocomposite Filaments for 3D Printing Application. Polymers (Basel). 2022, 14, 600.

50. Kazemi-Pasarvi, S.; Golshan Ebrahimi, N.; Shahrampour, D.; Arab-Bafrani, Z. Reducing cytotoxicity of poly (lactic acid)-based/zinc oxide nanocomposites while boosting their antibacterial activities by thymol for biomedical applications. Int. J. Biol. Macromol. 2020, 164, 4556–4565, doi:10.1016/j.ijbiomac.2020.09.069.

51. Oshani, B.N.; Davachi, S.M.; Hejazi, I.; Seyfi, J.; Khonakdar, H.A.; Abbaspourrad, A. Enhanced compatibility of starch with poly (lactic acid) and poly (ε-caprolactone) by incorporation of POSS nanoparticles: study on thermal properties. Int. J. Biol. Macromol. 2019, 141, 578–584.

52. Yang, S. lin; Wu, Z.H.; Yang, W.; Yang, M.B. Thermal and mechanical properties of chemical cross-linked polylactide (PLA). Polym. Test. 2008, 27, 957–963, doi:10.1016/j.polymertesting.2008.08.009.

53. Motelica, L.; Ficai, D.; Oprea, O.; Ficai, A.; Trusca, R.-D.; Andronescu, E.; Holban, A.M. Biode-gradable alginate films with ZnO nanoparticles and citronella essential oil—A novel antimicrobial structure. Pharmaceutics 2021, 13, 1020.

54. Thiyagu, T.T.; Uvaraja, G.G.V.C.; Arun, T.M.V.R. Effect of SiO 2 / TiO 2 and ZnO Nanoparticle on Cardanol Oil Compatibilized PLA / PBAT Biocomposite Packaging Film. 2022, 3795–3808, doi:10.1007/s12633-021-01577-4.

55. Khan, A.R.; Nadeem, M.; Aqeel Bhutto, M.; Yu, F.; Xie, X.; El-Hamshary, H.; El-Faham, A.; Ibrahim, U.A.; Mo, X. Physico-chemical and biological evaluation of PLCL/SF nanofibers loaded with orega-no essential oil. Pharmaceutics 2019, 11, doi:10.3390/pharmaceutics11080386.

56. Yasuniwa, M.; Tsubakihara, S.; Iura, K.; Ono, Y.; Dan, Y.; Takahashi, K. Crystallization behavior of poly(l-lactic acid). Polymer (Guildf). 2006, 47, 7554–7563, doi:https://doi.org/10.1016/j.polymer.2006.08.054.

57. Harris, A.M.; Lee, E.C. Improving the mechanical performance of injection molded PLA by controlling crystallinity. J. Appl. Polym. Sci. 2008, 107, 2246–2255.

58. Cipriano, T.F.; Silva, A.L.N. da; Silva, A.H.M. da F.T. da; Sousa, A.M.F. de; Silva, G.M. da; Rocha, M.G. Thermal, rheological and morphological properties of poly (lactic acid)(PLA) and talc compo-sites. Polímeros 2014, 24, 276–282.

59. Rodríguez-Tobías, H.; Morales, G.; Ledezma, A.; Romero, J.; Saldívar, R.; Langlois, V.; Renard, E.; Grande, D. Electrospinning and electrospraying techniques for designing novel antibacterial poly (3-hydroxybutyrate)/zinc oxide nanofibrous composites. J. Mater. Sci. 2016, 51, 8593–8609.

60. Yu, W.; Lan, C.-H.; Wang, S.-J.; Fang, P.-F.; Sun, Y.-M. Influence of zinc oxide nanoparticles on the crystallization behavior of electrospun poly (3-hydroxybutyrate-co-3-hydroxyvalerate) nanofibers. Polymer (Guildf). 2010, 51, 2403–2409.

61. Zhou, D.; Keller, A.A. Role of morphology in the aggregation kinetics of ZnO nanoparticles. Water Res. 2010, 44, 2948–2956, doi:10.1016/j.watres.2010.02.025.

62. Dadashi, P.; Babaei, A.; Abdolrasouli, M.H. Investigating the hydrolytic degradation of PLA/PCL/ZnO nanocomposites by using viscoelastic models. Polym. Eng. Sci. 2022, 62, 869–882, doi:10.1002/pen.25893.

63. Liu, L.; Jin, T.Z.; Coffin, D.R.; Hicks, K.B. Preparation of antimicrobial membranes: coextrusion of poly (lactic acid) and nisaplin in the presence of plasticizers. J. Agric. Food Chem. 2009, 57, 8392–8398.

64. Lu, W.; Cui, R.; Zhu, B.; Qin, Y.; Cheng, G.; Li, L.; Yuan, M. Influence of clove essential oil immobilized in mesoporous silica nanoparticles on the functional properties of poly (lactic acid) biocompo-site food packaging film. J. Mater. Res. Technol. 2021, 11, 1152–1161.

65. Li, Y.; Liu, Y.; Campos de Souza, S.; Chao, T.; Dong, L.; Sun, G.; Wang, C.; Niu, Y. Differential Foreign Body Reactions between Branched and Linear Glucomannan Scaffolds. J. Funct. Biomater. 2022, 13, doi:10.3390/jfb13040293.

66. Stieglitz, T.; Schuettler, M. Material-tissue interfaces in implantable systems; Woodhead Publishing Limited, 2013; ISBN 9781845699871.

67. Mariani, E.; Lisignoli, G.; Borzì, R.M.; Pulsatelli, L. Biomaterials: Foreign bodies or tuners for the immune response? Int. J. Mol. Sci. 2019, 20, doi:10.3390/ijms20030636.

68. Barral, V.; Dropsit, S.; Cayla, A.; Campagne, C.; Devaux, É. Study of the influence of pcl on the in vitro degradation of extruded pla monofilaments and melt-spun filaments. Polymers (Basel). 2021, 13, 1–15, doi:10.3390/polym13020171.

69. Laurenti, M.; Cauda, V. ZnO nanostructures for tissue engineering applications. Nanomaterials 2017, 7, doi:10.3390/nano7110374.

70. Xu, N.; Lei, H.; Li, X.; Wang, Q.; Liu, M.; Wang, M. Protective effects of ginger essential oil (Geo) against chemically-induced cutaneous inflammation. Food Sci. Technol. 2019, 39, 371–377, doi:10.1590/fst.14318.